5-5-2017

Hydrogel-based Conductive Polymers for Nerve Regeneration

Scott R. Stratton
University of Connecticut - Storrs, scott.stratton@uconn.edu

Hydrogel-based Conductive Polymers for Nerve Regeneration

Scott Ryan Stratton

B.S., University of Connecticut, 2015

A Thesis

Submitted in Partial Fulfillment of the

Requirements for the degree of

Master of Science

At the

University of Connecticut

2017

Approval Page

Master of Science Thesis

Hydrogel-based Conductive Polymers for Nerve Regeneration

Presented by

Scott Ryan Stratton, B.S.

Major Advisor _____
Sangamesh G. Kumbar, Ph.D.

Associate Advisor _____
Syam P. Nukvarapu, Ph.D.

Associate Advisor_____
Wendy Vanden Berg-Foels, Ph.D.

University of Connecticut

2017

Acknowledgements

I wish to acknowledge Dr. Sangamesh Kumbar and his laboratory for giving me the resources necessary to complete my thesis work, and all of the faculty and staff at the University of Connecticut for supporting me over the course of this study. I would also like to acknowledge funding from The Raymond and Beverly Sackler Center for Biomedical, Biological, Physical and Engineering Sciences as well as funding from National Science Foundation Award Number IIP-1311907, IIP-1355327; and EFRI-1332329, and the Department of Defense (OR120140).

Table of Contents

Abstract

Autografts and allografts have been deemed the “gold standard” for nerve regeneration due to their ability to regenerate peripheral nerve gaps beyond biological limits. However, drawbacks associated with these methods include donor site morbidity, risk of neuroma, lack of control over scar formation, and risk of an immune response. As such, tissue engineering has developed new methods to bridge nerve gaps, such as nerve guidance conduits (NGCs) seeded with stem cells. Used in conjunction with electrical stimulation (ES) in place of costly growth factors, wound healing is further accelerated. Ionically conductive polymeric substrates containing sulfonated polyaniline (SPANI) and lignin sulfonate (LS) are characterized in physiological conditions and later seeded with human mesenchymal stem cells (hMSCs). Following treatment with ES at 1V and 20kHz over a 14 day period, viability, differentiation, and proliferation are observed. In comparison to positive control nerve growth factor (NGF), ES was demonstrated to be a viable candidate for regulating cellular behavior.

1. Introduction

Peripheral nerve damage is a significant concern worldwide, affecting a wide variety of people from all different types of socioeconomic backgrounds and cultures (*1, 2*). This is largely due to the limitations of peripheral nerve tissue to spontaneously regenerate itself past 5mm gaps (*3*). Thus, the traditional treatment for the regeneration of nerve tissue has consisted of autographs and allografts (*4*). However, the drawbacks of these conventional methods for nerve repair include a possibility of donor site morbidity, risk of an immune response, risk of neuroma, recurring pain, and lack of control over scar tissue formation (*5-7*). Conventional methods also place an economic burden on society as it is estimated that nearly $150 billion is spent annually in the United States alone on nerve repair procedures (*6*).

In recent years, novel tissue engineering approaches have been taken in attempt to counteract many of the drawbacks of traditional methods for nerve repair. In particular, nerve guidance conduits (NGCs) have become largely popularized, using a variety of different biomaterials and fabrication methods (*8*). These tubular structures not only counteract the disadvantages of traditional methods, but also provide several advantages of their own. Control over degradation rate, allowing for steady release of growth factors, and a wide variety of biomaterials to choose from for fine-tuning of mechanical properties are a few such advantages (*9, 10*). In addition, NGCs provide a channel for the guided outgrowth of nerve in one particular direction, preventing the spread of several axons in different directions (*5*).

Conduits made of electrospun nanofibers have largely been explored in the past few years (*11, 12*). Electrospun polycaprolactone (PCL) composite matrices have been used for nerve regeneration applications, due to the elastic mechanical properties of PCL, which mimic those of native nerve tissue, and interconnected porosity resembling the extracellular matrix (ECM) (*13*).

However, PCL is too hydrophobic to allow for sufficient cellular adhesion by itself and has a relatively slower degradation rate than desired for most nerve regeneration applications (*14, 15*). For this reason, PCL is often blended with hydrophilic biomaterials that are known to promote cellular adhesion or finely tune degradation rate (*16, 17*). For example, cellulose acetate (CA) has shown promising results as a biocompatible material for scaffolding in recent years due to its tensile strength and hydrophilic nature for cellular compatibility, making it an ideal candidate for blending with PCL (*18, 19*).

In addition to being supportive of cellular attachment and ECM mimicry, conductivity has also been shown to be an important factor for bridging nerve gaps due to the remarkable ability of nerve gaps to recover beyond biological limits in the presence of an electrical charge (*20*). Electrical stimulation (ES) studies have received spotlight for ability to promote Schwann cell outgrowth, increase nerve branching when compared to control groups without ES, and speculation that stem cells may differentiate into neuronal lineages in the presence of conducting polymers with applied ES (*21-23*). ES has gained further attention due to the fact that it provides a viable alternative to growth factors, which NGCs are often loaded with, in order to regulate cellular behavior (*24*). There is now a need for an alternative as growth factors present an unideal, short half-life and costly economic burden (*25*).

Research, however, is lacking on the viability of conductive polymers for nerve regeneration applications. Lignin polymeric composites, for example, have demonstrated biological compatibility by promoting cellular proliferation, attachment, and interaction of human dermal fibroblasts *in vitro* (*26*). Yet, the viability of such scaffolds for nerve regeneration applications in the presence of ES has yet to be determined. Other biomaterials also have shown to be viable candidates to form PCL nanofiber composites for nerve regeneration applications,

such as sulfonated polyaniline (SPANI). SPANI is shown to enable cellular viability similar to that of other well-known biocompatible polymers such as poly(L-lactic) acid (PLLA), and presents an ionically charged sulfonic group which paves the way for high conductivity (*27*). However, once again, research is lacking on the effects that SPANI may have on cellular proliferation and differentiation in the presence of ES.

In order to address the need for a conductive NGC which is supportive of cellular attachment, randomly orientated PCL/CA (80:20) nanofibers are fabricated into composite scaffolds by coating with three different hydrogel composites – 3wt% chitosan (CHT), 20wt% SPANI in 3wt% CHT, and 20wt% lignin sulfonate (LS) in 3wt% CHT. Characterization techniques are performed in order to evaluate the material composition of each scaffold.

Mechanical testing is performed as well as a weight loss study, followed by conductivity analysis over an 8 week period in 7.4pH phosphate buffer saline (PBS) with additional thermogravimetry analysis (TGA). Human-derived mesenchymal stem cells (hMSCs) are then seeded onto each scaffold and viability and differentiation are examined for all groups. A PicoGreen DsDNA assay is used to observe proliferation in ES groups over a 14 day period. ES is performed at 1V with 20kHz daily.

The hypothesis of this study is that hydrogel-coated PCL/CA nanofibers blended with conductive polymers will demonstrate biologically relevant material properties and provide an environment suitable for cell attachment, proliferation, and differentiation for nerve regeneration applications with the use of ES.

2. Materials and Methods

2.1 Preparation of Samples

2.1.1 Fabrication of PCL/CA nanofibers

Briefly, 10wt% PCL with 2.5wt% CA (80:20 ratio) was prepared in 10mL solution containing 1g of PCL beads, 0.25g of CA, 8.5mL of dichloromethane (DCM), and 1.5mL of ethanol in a scintillation vial. The solution was left overnight to stir. The next day, 6mL of solution was placed into an 18-gauge needle for electrospinning. Electrospinning was performed at 2.5mL per hour, with a distance of 20cm from the needle tip to the collector and a diameter of 12.4mm. The applied voltage was 15kV with DC current.

2.1.2 Preparation of SPANI

5mL of aniline was prepared in a scintillation vial and mixed with 1.35g of propane sultone at room temperature for 6 hours to form sulfonated aniline, dissolved in acetone and left overnight. The following day, the solution is filtered until the acetone is removed completely. Then, persulfate is added in a 1:1 ratio, the entire solution is dissolved in water and finally left at room temperature in order to polymerize SPANI. Dialysis is performed, changing the water when necessary, and finally storing in liquid nitrogen before lypholysis is performed in order to remove excess liquid and leave SPANI.

2.1.3 Preparation of composite nanofibers

Starting with the procedure outlined by Shelke et al. (*15*), 3wt% solution of CHT was prepared by pouring 3g of CHT into a 100mL scintillation vial of water while stirring and left stirring overnight. Similarly, 20wt% solution of LS was prepared by moving 10mL of the CHT/water solution into a separate scintillation vial and adding 0.06g (approximately 20% of 0.3g/10mL of CHT) of LS while stirring. The solution was once again left stirring overnight. The procedure followed once again for the 20wt% SPANI in 3wt% CHT solution – 10mL of the

CHT/water solution was placed into a separate scintillation vial and 0.06g of SPANI was added while stirring. Afterwards, the solution was left stirring overnight.

2.2 *In Vitro* Characterization

2.2.1 Fourier transform-infrared spectroscopy (FTIR) analysis

Each of the four groups were characterized using FTIR. FTIR analysis was performed at 32 scans in the wavelength range of 4000cm^{-1} to 500cm^{-1} while pressing samples against the crystal. Analysis was done at room temperature using Thermo Scientific Smart FTIR technology.

2.2.2 Scanning electron microscopy (SEM) analysis

SEM technology is used to examine the micro-scale hydrogel coating of the fibrous samples and note any distinct structural characteristics. SEM is performed using JEOL 6335F FESEM (Boston, MA, USA) at 20kV operating voltage and 1000X magnification. Samples were sputter coated with gold using Hummer V sputtering system (Technics Inc., Baltimore, MD) before placement on the microscope for imaging.

2.2.3 Weight loss in physiological conditions

In order to examine the percent weight loss over time due to leeching of polymeric material, samples were submerged in PBS at day 0 and weighed for 25 days. PBS was changed every other day in order to maintain a consistent concentration gradient. Over time, the samples were weighed after longer time intervals as their masses stabilized.

2.2.4 Mechanical testing

Samples were submerged overnight in PBS solution in preparation for mechanical testing the following day. In accordance with established ASTM guidelines, each of the four groups were cut into dog bone-like shapes measuring 20mm by 10mm (length/breadth) and subjected to a tensile force at both ends at 10mm/min until the samples reached failure. The test equipment used was Instron 5544, Norwood MA.

2.2.5 Conductivity analysis in physiological conditions

Similar to weight loss analysis, samples measuring 2 inch by 2 inch are immersed in 7.4pH PBS and the media is routinely changed. Three samples from each of the four groups are taken and stored at 4ºC at time points day 1, 1 week, 2 weeks, 4 weeks, and 8 weeks. For conductivity analysis, samples are re-immersed in PBS for one minute before resistance is measured using two-point contact. The equipment used to measure resistance is an ohmmeter (Keithlay Integra Series 2700.) Electrical conductivity α is calculated as $\alpha = \frac{L}{RA}$, where L is the thickness of the sample, R is the noted resistance, and A is surface area.

2.2.6 TGA analysis in physiological conditions

TGA analysis is performed using TGA Q-500 (TA Instruments, New Castle, DE). For each dry sample, 10mg is weighed and analysis is performed in air gas, ranging from temperatures 10°C to 800°C with an equilibrium temperature of 200°C. Universal Analysis software (TA instruments, New Castle, DE) is used to obtain waveforms corresponding to percent initial weight as a function of temperature. Samples are immersed in PBS solution at 37°C for a 4 week period and analysis is performed at day 0 (pre-immersion) and week 4.

2.3 Cell Study

2.3.1 Cell seeding

Human mesenchymal stem cells (hMSCs) from Lanza (CAT#PT-2501) were expanded *in vitro* on the third passage using Dulbecco's Modified Eagles Medium (DMEM, CAT#12-604F BioWhittaker® Lonza, Walkersville, MD) supplemented along with 10% fetal bovine serum (FBS, CAT#10437028 Gibco, Grand Island, NY) and 1% penicillin/streptomycin (P/S, CAT#15140122 Gibco, Grand Island, NY). Media was changed every other day. The hMSCs were once again expanded on the fourth passage at 80% confluency. Samples were seeded statically at 20,000 cells per scaffold on the fifth passage at 80% confluency. Cells were pipetted directly on top of each sample in a sterile 24 well plate and left in the incubator for 4 hours in

order to allow for cell attachment. Next, 200µL of media was later placed in each well and changed every other day. Prior to seeding, samples were immersed in media for 2 hours in order to allow for infiltration of growth factors and nutrients. Sterilization of the samples was performed by immersion in 70% ethanol solution for approximately 20 minutes, followed by exposure to UV for 35 minutes on each side.

2.3.2 Cell treatment with NGF

Based on the differentiation research performed by Bellot et al., the growth factor groups were treated with 70ng/mL of NGF solution (Murine, natural, 2.5S Gibco, Grand Island, NY) every other day, corresponding to each media change (*28*). Treatment was begun at day 0 and continued until day 14.

2.3.3 Cell treatment via ES

While ES has become popularized in recent years for nerve regeneration applications, no established protocol exists to date. Voltage, frequency, and duration of stimulation vary widely in literature. For this particular study, the parameters used are either 1V at 20kHz for 10 minutes per day. The electrodes used are in the form of a positively charged gold ring touching the outer edges of the sample with a ground ring touching the center, such that current travels from the outer edges toward the center in response to a voltage difference.

2.3.4 Live/dead assay (cellular viability)

A live/dead assay is conducted by rinsing samples in PBS twice, followed by incubation at room temperature with 0.05% calcein, AM at 494/517nm and 0.2% ethidium bromide at 528/617nm (CAT#L3224 Life Technologies, Eugene, Oregon). Samples are observed using a confocal microscope. Ethidium bromide penetrates the membranes of dead cells and excitation occurs upon binding to nucleic acids, while calcein excites upon binding to esterase in the intracellular environment.

2.3.5 Immunohistochemistry (cellular differentiation)

For immunostaining, samples are fixed for 30 minutes with 4% paraformaldehyde (Sigma, St. Louis, MO) in 7.4pH PBS solution after removing media completely. Samples are then washed with PBS 3 times, followed by permeabilizing in 0.2% Triton X-100 in PBS for 10 minutes at room temperature. Once again, samples are washed with PBS 3 times, and then non-neuronal proteins are blocked by incubating with 1% bovine serum albumin (BSA) in PBST (PBS with 0.1% Tween 20) for 30 minutes at room temperature. Again, samples are washed with PBS 3 times. The primary neuronal antibodies, anti-rabbit microtubule-associated protein 2 (MAP2, Abcam, Cambridge, MA) and anti-mouse β-III Tubulin (Abcam, Cambridge, MA), are diluted in 1:200 and 1:1000 ratios in 1% BSA in PBST respectively, and 150μL is placed on each sample. Samples are incubated with primary antibody solution overnight at 4°C. The following day samples are washed 3 times with PBS followed by incubation for 1 hour with secondary antibodies, Rhodamine Red (goat anti-rabbit) and Alexa Flour 488 (goat anti-mouse), in 1:100 ratios and carefully protected from light. Lastly, samples are washed with PBS 3 times prior to viewing via confocal microscopy.

2.3.6 PicoGreen dsDNA assay (cellular proliferation)

Cellular proliferation is analyzed for scaffolds treated with ES at days 1, 7, 11, and 14 using a PicoGreen dsDNA assay kit (P7589, Life Technologies). Scaffolds (N=3) are collected at their respected time points, washed twice with PBS in order to remove culture media, and then frozen with 600μL of 1% triton X-100 solution in distilled water. Scaffolds were thawed and re-frozen at least twice in order to ensure complete lysing of the membrane, followed by mixing of the scaffold-triton X-100 solution using a standard rocker. In a 96 well plate, 20μL of cell suspension is placed in each well with 80μL of provided 1X TE buffer solution and provided PicoGreen reagent in TE buffer with 20X dilution. After immediate covering of the plate in order

to prevent light penetration, samples were incubated at room temperature for 5-10 minutes and then read using a BioTek (Synergy HT) plate reader at 485nm emission and 535nm excitation. A standard curve was used to determine DNA concentration in each scaffold.

2.4 Statistical analysis

Quantitatively displayed data is reported in terms of mean ± standard deviation, except PicoGreen which is reported in terms of mean ± standard error. One-way ANOVA analysis is also performed with significance being reported in results in which $p>0.05$.

3. Results and Discussion

While growth factors have typically performed the role of regulating cellular behavior for wound healing applications, particularly when loaded onto NGCs, they suffer from drawbacks including an economic burden and short half-life (*25*). Thus, there is a clinically unmet need for a viable alternative. ES has been demonstrated as this potential alternative, as performance on animal models for *in vivo* nerve regeneration applications have been shown to accelerate the bridging of nerve gaps in the PNS beyond traditional biological limits (*29*). This is largely due to the fact that ES promotes the outgrowth of Schwann cells post-injury and induces accelerated ECM production (*21, 30*).

Thus, the objective of this study was to develop a novel, ionically conductive material for use as a NGC and characterize it for biological relevance and cellular behavior under the influence of applied ES in comparison to NGF.

3.1 Characterization Techniques

3.1.1 FTIR spectra analysis

PCL has been well characterized as a biodegradable polymer and composite material (*31-34*). It is has been demonstrated that there is a peak in its FTIR spectra correlating with a wavelength of 1724cm^{-1} for the ester carbonyl functional group (*35*), as can be observed in *figure*

1. The presence of CA is also demonstrated by a methyl functional group corresponding to a wavelength of 1370cm^{-1} (*36*). For all hydrogel groups, the presence of chitosan is noted both by the presence of amine groups (*37*) at 1650cm^{-1} and OH and NH bonds between 3357cm^{-1} and 3284cm^{-1} (*38*). Lastly, for the PCL/CA+CHT/LS and PCL/CA+CHT/SPANI groups, the presence of the ionically conductive polymers is noted by a sulfonated aromatic ring at 1070cm^{-1} (*39*).

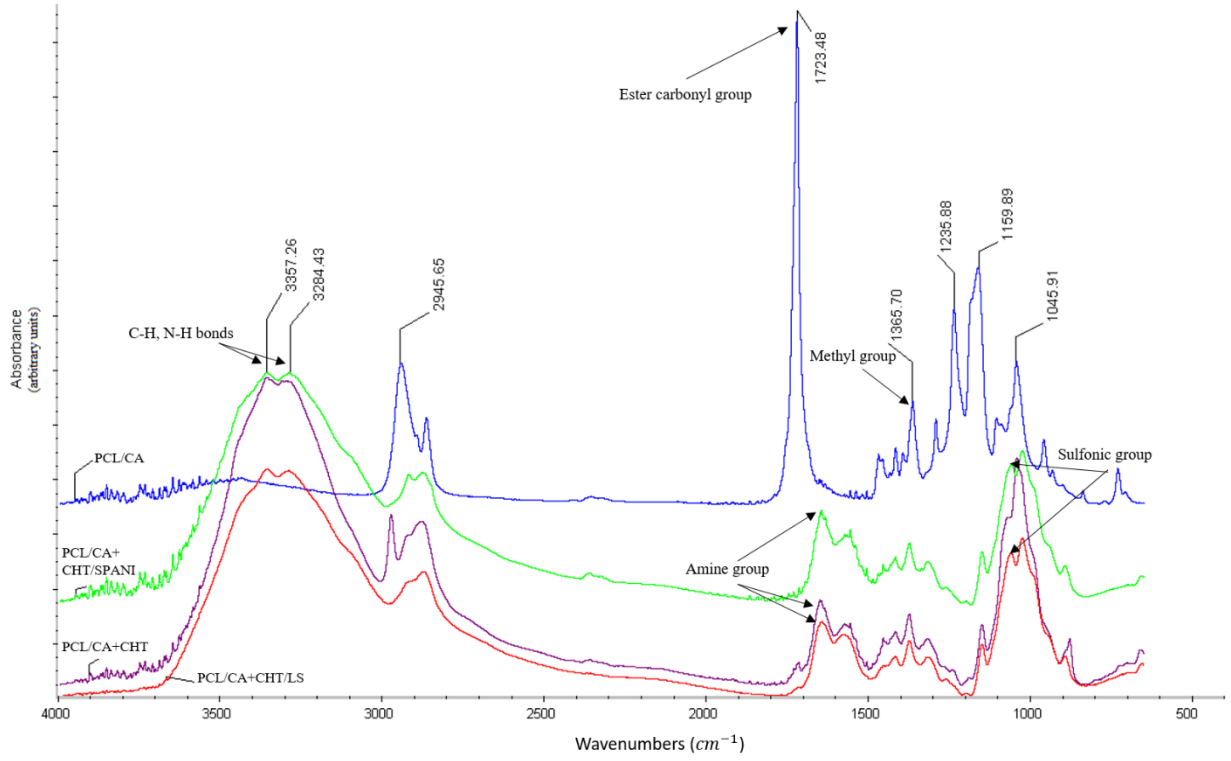

FIG. 1. FTIR spectra analysis is shown above. It can be observed that the absorbance peaks in the PCL/CA group, indicated by the blue waveform, correspond to a wavelength of approximately 1723.48cm^{-1} for the C=O bonds of the ester carbonyl group of PCL, and 1365cm^{-1} for the methyl group of CA. The absorbance peaks in the PCL/CA+CHT group, indicated by the purple waveform, demonstrate a suppression of the ester carbonyl group, proving that the hydrogel coating is present. Additionally, there are peaks at1650cm^{-1} corresponding to the N-H amine bonds of Chitosan and between 3357.26cm^{-1} and 3284.43cm^{-1} corresponding to the O-H, N-H bonds of chitosan. Lastly, there are peaks corresponding to sulfonated aromatic rings at 1070cm^{-1} in the PCL/CA+CHT/LS and PCL/CA+CHT/SPANI groups, demonstrating the presence of the ionically conductive sulfonic groups in both conductive polymers.

3.1.2 SEM analysis

The role of the extracellular matrix is to provide a porous environment suitable for nutrient transportation, cell signaling, and regulation of stem cell fate (*40*). Thus, the PCL/CA

nanofibers should be randomly orientated in order to give way to interconnected porosity. As can be observed in *figure 2*, part (A) demonstrates an SEM surface view of the PCL/CA group at 1000X magnification and 20kV. The interconnected porosity formed by randomly orientated fibers can be seen. Parts (B), (C), and (D) represent the PCL/CA+CHT, PCL/CA+CHT/LS, and PCL/CA+CHT/SPANI groups respectively. The hydrogel coating can be observed over the nanofiber matrix.

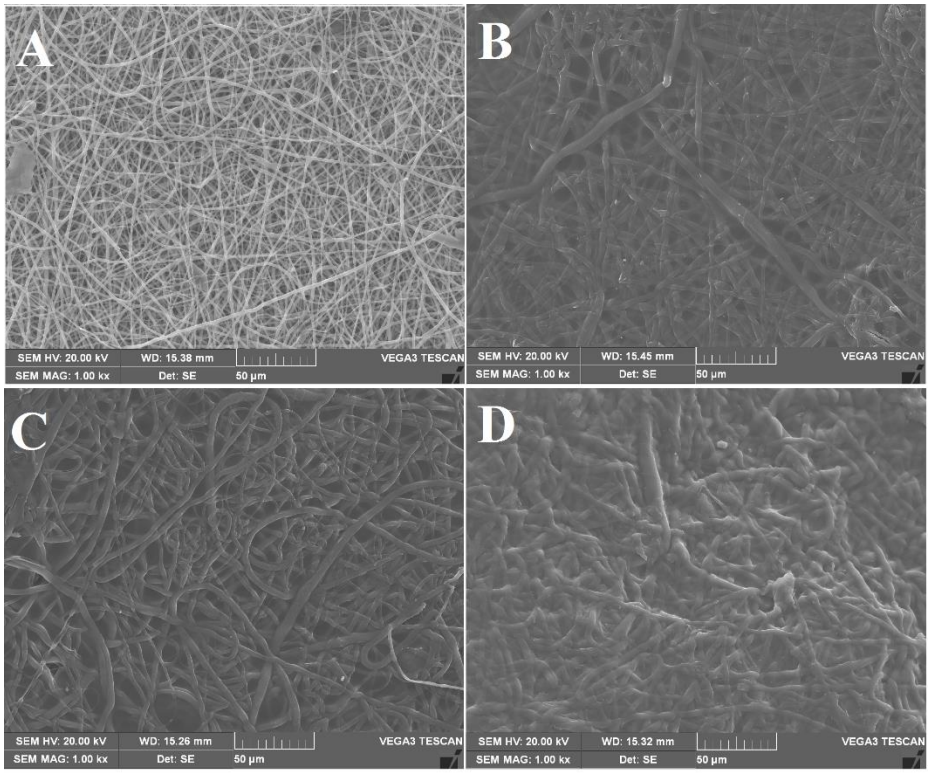

FIG. 2. SEM technology is used to characterize the hydrogel-based scaffolds at 20kV and 1000X magnification. Part (A) shows the non-coated PCL/CA nanofibers in a random orientation, part (B) shows the PCL/CA+CHT composites as the coating of the fibers can be noted, and parts (C) for PCL/CA+CHT/LS and (D) for PCL/CA+CHT/SPANI additionally confirm the hydrogel coating of the PCL/CA nanofibers.

3.1.3 Weight Loss analysis in physiological conditions

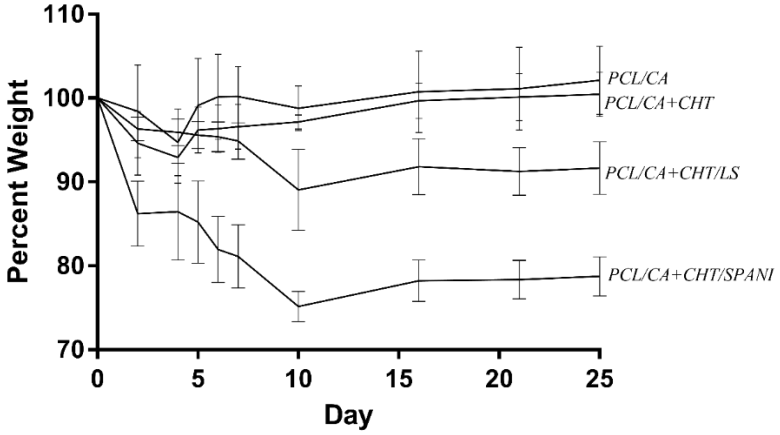

FIG. 3. It can be observed that PCL/CA+CHT/SPANI had the greatest weight loss due to polymeric leeching with only 78.76%±2.35% of its initial weight left after 25 days , followed by PCL/CA+CHT/LS at 91.64%±3.14%. PCL/CA and PCL/CA+CHT were relatively constant throughout at 102.11%±4.07% and 100.45%±2.64% of initial weight respectively after 25 days. It is theorized that the reason for this phenomena is the greater hydrophilicity of SPANI.

3.1.4 Tensile properties

The brittle nature of CHT as a biomaterial has been documented (*41*), in addition to the elastic nature of PCL (*42*). CHT is expected to swell in aqueous conditions as a hydrogel causing a mechanical stretching of the polymeric bonds (*43*). CA by itself has been shown to demonstrate brittle properties, and for this reason is often blended with other materials for greater biologically relevant elasticity (*44*).

When samples are immersed in 7.4 pH PBS overnight and subjected to a tensile test, the findings of this study are in agreement with those in literature. *Figure 4* demonstrates the tensile strength of each scaffold group, in addition to pure PCL, and *figure 5* demonstrates the corresponding modulus of elasticity. As expected from observation of *figure* 4, the tensile strength is significantly lower in the hydrogel coated groups when compared to the nanofiber groups due to well documented swelling characteristics causing a premature mechanical stretching of the polymeric bonds when immersed in 7.4pH PBS. Additionally, the PCL/CA group is shown to exhibit greater tensile strength in comparison to the pure PCL counterpart.

Also as expected from observation of *figure 5*, the PCL/CA nanofiber blend is less elastic in nature when compared to pure PCL nanofibers, and the CHT hydrogel groups are more brittle in nature when compared to solely nanofiber groups.

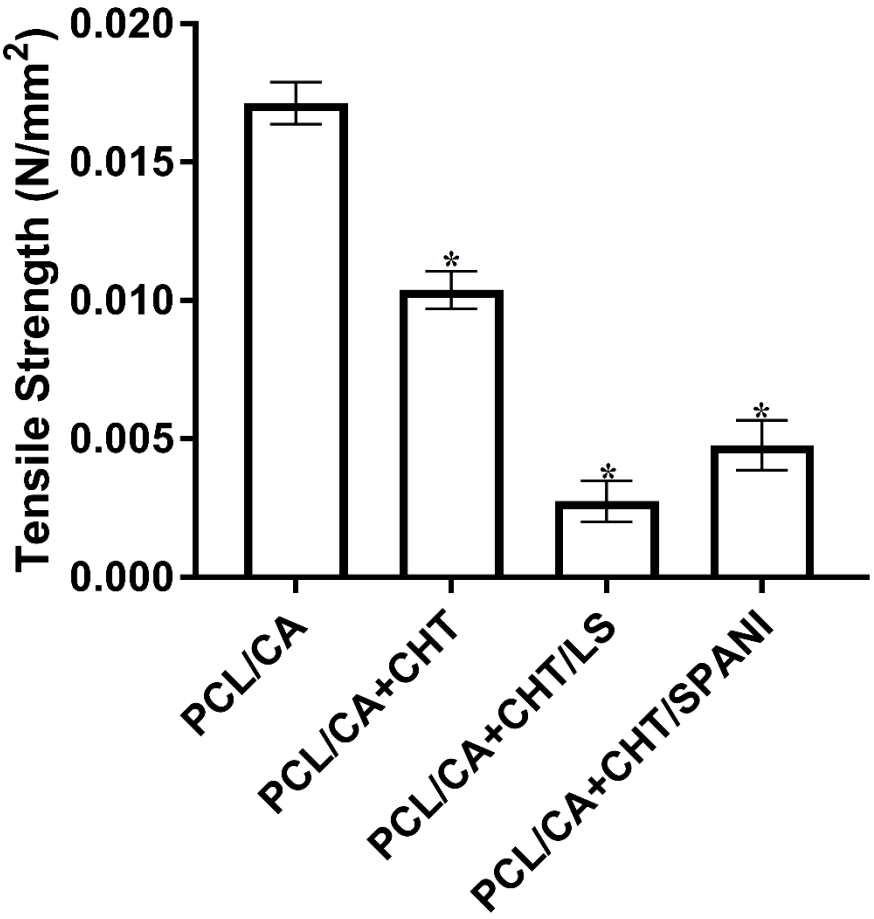

FIG. 4. It can be observed that PCL/CA demonstrates the highest tensile strength, followed by PCL/CA+CHT, then pure PCL, with PCL/CA+CHT/LS and PCL/CA+CHT/SPANI enduring the least load. The reason proposed for this phenomena is that, with increasing load density, the fibers are already pre-stretched upon swelling due to immersion in PBS for 24 hours. *Indicates $p<0.05$ versus PCL/CA.

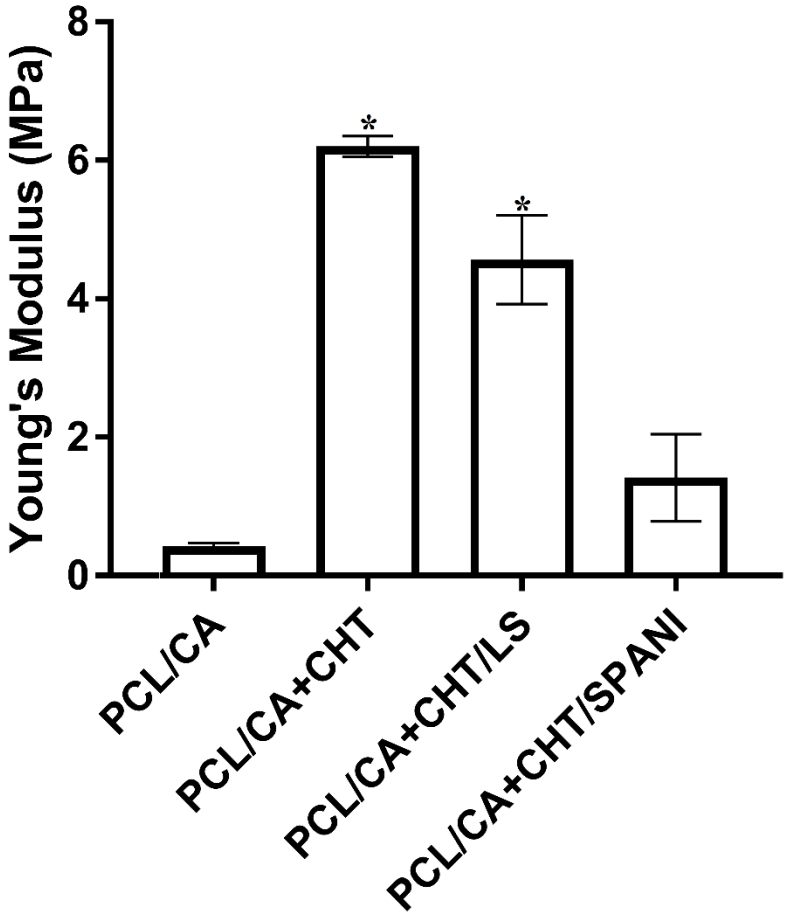

FIG. 5. It can be observed that the Young's Modulus was greatest for PCL/CA+CHT, followed by PCL/CA+CHT/LS and PCL/CA+CHT/SPANI, and lastly PCL/CA followed by pure 12.5% PCL. It is theorized that the reasoning behind this phenomena is the brittle nature of the crosslinked CHT bonds in combination with already pre-stretched fibers. The LS and SPANI groups most likely had a lower modulus due to a slight breaking of the PCL/CA fibers bonds upon CHT swelling in PBS solution. *Indicates $p<0.05$ versus PCL/CA.

3.1.5 Conductivity analysis in physiological conditions

Because of the potential for nerve regeneration in the PNS in the presence of ES (*45*) as well as the economic burden and short half-life of growth factors (*46*), conductivity is now an important factor for NGCs. The lack of conductivity of PCL is well understood, and thus researchers have attempted to improve this parameter by fabricating composites with other materials (*47*).

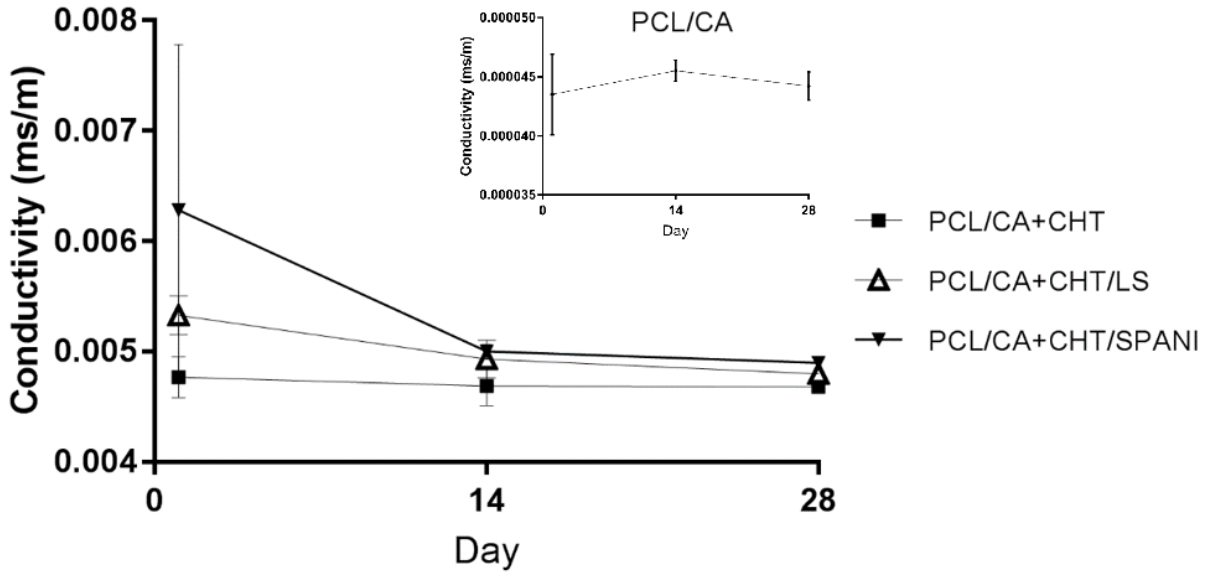

FIG. 6. The conductivity of the each group is analyzed at days 1, 14, 28. As expected, the matrices maintain most of their conductivity within the margin of error following immersion in 7.4pH PBS at 37ºC.

3.1.6 TGA analysis in physiological conditions

Researchers have used TGA analysis extensively to characterize the thermal degradation of composite materials (*48-51*). For instance, Gil et al. demonstrated that both sterilization methods and percent concentration of silk biomaterial-based scaffolds has a direct effect on their TGA curves (*52*). Moreover, Kolmas et al., have demonstrated that varying the composition of nanocrystalline apatite material for bone regeneration applications influences the characteristic TGA curve due to the molecular weights of the individual polymers (*53*).

Within the context of this study, samples were immersed in PBS solution at 37°C for a period of 4 weeks. Samples weighing 10mg from each group are then heated in air gas from 10°C to 800°C with a 200°C equilibrium temperature. If a significant amount of polymeric material was lost during this time period due to degradation or diffusion, there should therefore be a noticeable qualitative difference in the TGA curves generated from day 0 (pre-immersion) in comparison to 4 weeks. On this hypothesis, there should be significant qualitative differences for the PCL/CA, PCL/CA+CHT, PCL/CA+CHT/LS, and PCL/CA+CHT/SPANII groups' TGA

curves over time if polymeric material was in fact lost. The resulting TGA analysis indicated that there was little to no qualitative difference noted. These results are depicted in *Figure 8*, which provides a view of these generated curves for each sample. Parts (A) and (B) represent the PCL/CA group at day 0 and week 4 respectively, while parts (C) and (D) represent the PCL/CA+CHT group, parts (E) and (F) represent the PCL/CA+CHT/LS group, and lastly parts (G) and (H) represent the PCL/CA+CHT/SPANII group. With the exception of some small weight retention starting at 600°C at 4 weeks, there is no significant qualitative different noted with each of the curves. The phenomena of weight retention is most likely explained due to salt concentration in the PBS solution, which diffuses into the interconnected pores of the scaffolds.

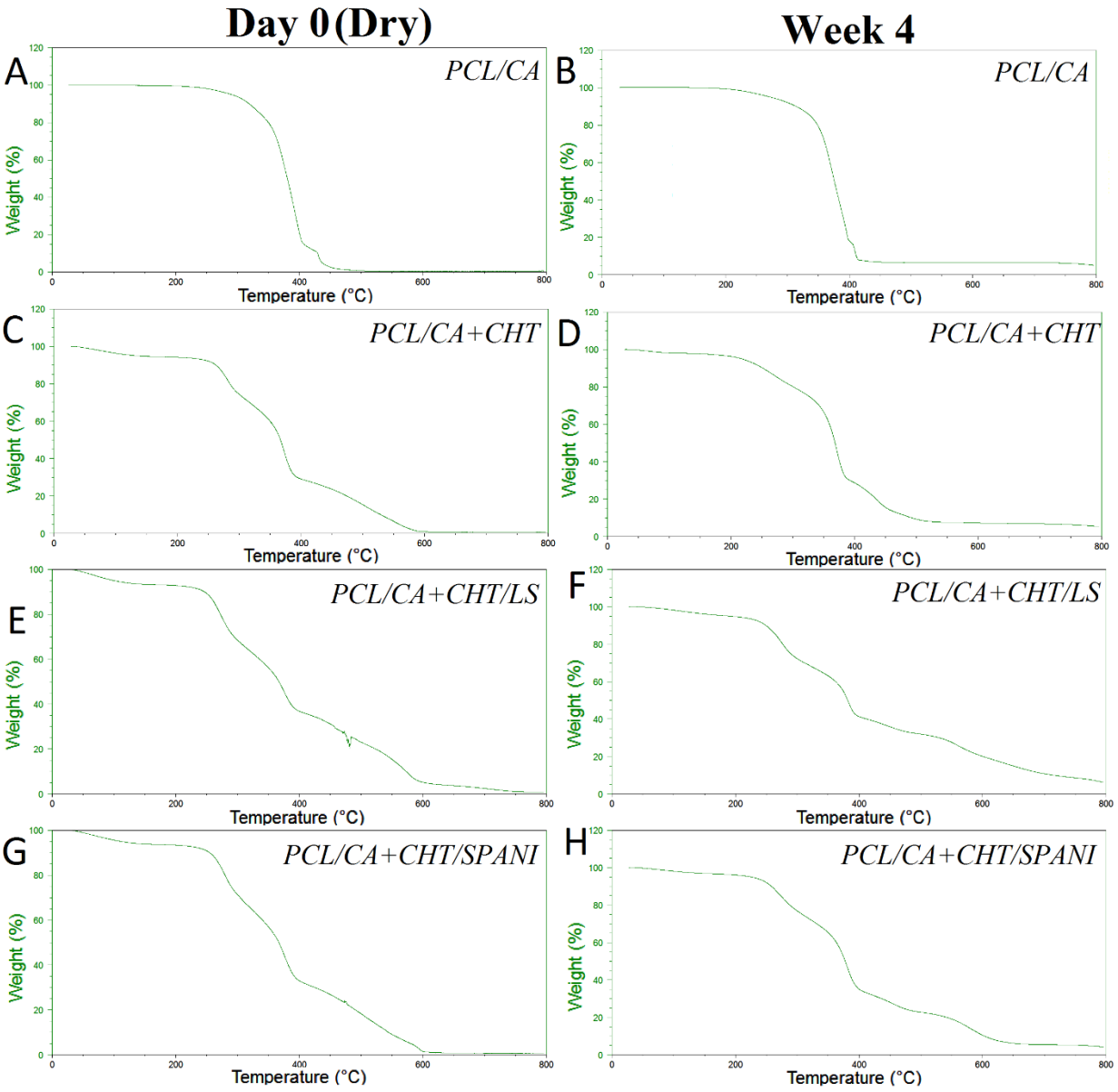

FIG. 8. TGA analysis is performed for each of the 4 sample groups at day 0 (pre-immersion in PBS at 37°C) and week 4 (post-immersion in PBS at 37°C). Parts (A) and (B) represent the PCL/CA group at day 0 and week 4 respectively, while parts (C) and (D) represent the PCL/CA+CHT group, parts (E) and (F) represent the PCL/CA+CHT/LS group, and lastly parts (G) and (H) represent the PCL/CA+CHT/SPANII group. As can be noted from observation of the characteristic weight loss profiles, samples at week 4 retain slightly more weight in comparison to their day 0 counterparts. This phenomena is most likely accounted for by an intake of salt concentrations present in the PBS solution, which is retained up to 800°C.

3.2 Cell Study

For cell studies, samples are cut into a circular shape with 11mm diameter, as can be observed in *figure 9*, showing each of the four groups. Samples are placed into a 24 well plate after sterilization via immersion in 70% ethanol for 15 minutes and UV radiation for 35 minutes on each side. Media is changed every other day and ES takes place at 1V, 20kHz, and 10 minutes per day.

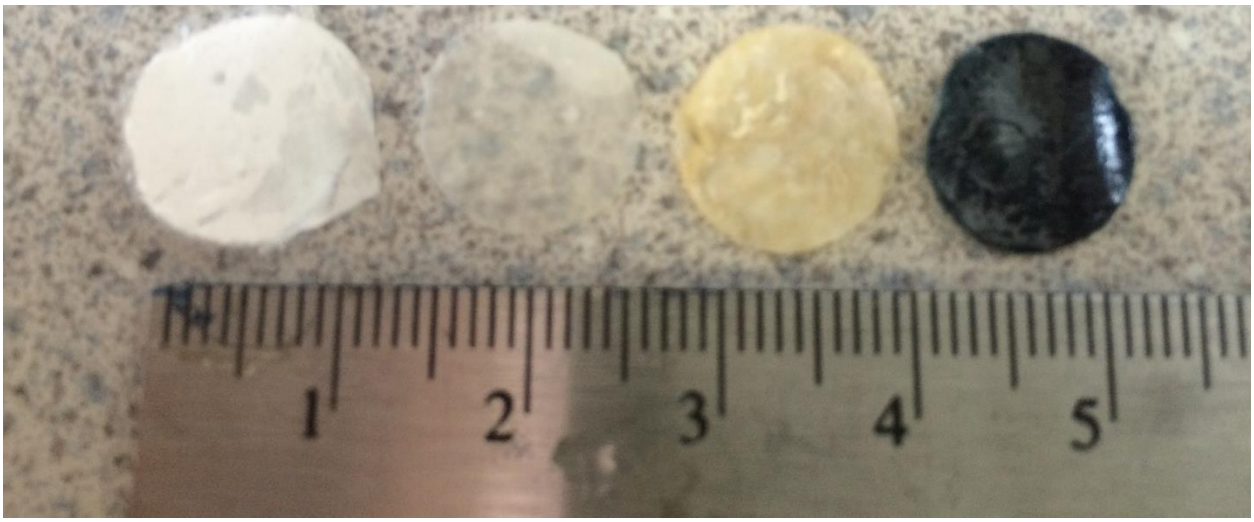

FIG. 9. For *in vitro* cell studies, samples are cut into circular shapes measuring 11mm in diameter. From right to left, the groups of PCL/CA, PCL/CA+CHT, PCL/CA+CHT/LS, and PCL/CA+CHT/SPANI can be noted.

3.2.1 Cell viability

PCL is too hydrophobic in nature to allow for desired cellular attachment on its own, and thus is often blended with other polymers that are more hydrophilic in nature (*54*). CA fulfills this blending need, demonstrating both cellular attachment and proliferation profiles (*55*). Therefore, PCL was blended with CA in an 80:20 ratio. For all 3 hydrogel groups, it should be noted that CHT, lignin, and polyaniline (PAN) have all been demonstrated to be supportive of cell attachment and viability with the possibility of further functional group modification (*26, 56, 57*). *Figure 10* demonstrates the expected result of cell seeding onto these 4 groups when observed at day 14 via confocal microscopy. Part (A) represents the PCL/CA group, part (B)

represents the PCL/CA+CHT group, part (C) represents the PCL/CA+CHT/LS group, and part (D) represents the PCL/CA+CHT/SPANI group. It can be observed, as indicated by green staining, that the scaffolds are supportive of cell attachment and viability over a 14 day period for both NGF and control groups, and at least an 11 day period for ES treatment. While there are little to no cells observed in ES groups at day 14 (data not shown), it is worth noting that the presence of hMSCs or Schwann cell lineages at least until day 11 has been shown to be important for macrophage recruitment and cell signaling, stimulating wound healing beyond biological limitations through formations such as the bands of Büngner (*58-60*).

Axonal-like and dendritic-like morphological changes have been well documented in stem cells in the process of differentiating into neuronal lineages (*61-63*). Therefore, it is expected that in the presence of NGF such morphological changes should be noted on each scaffold group. Observation of *figures 11* and *12* in comparison to *figure* 10 reveals axonal and dendritic-like structures emerging.

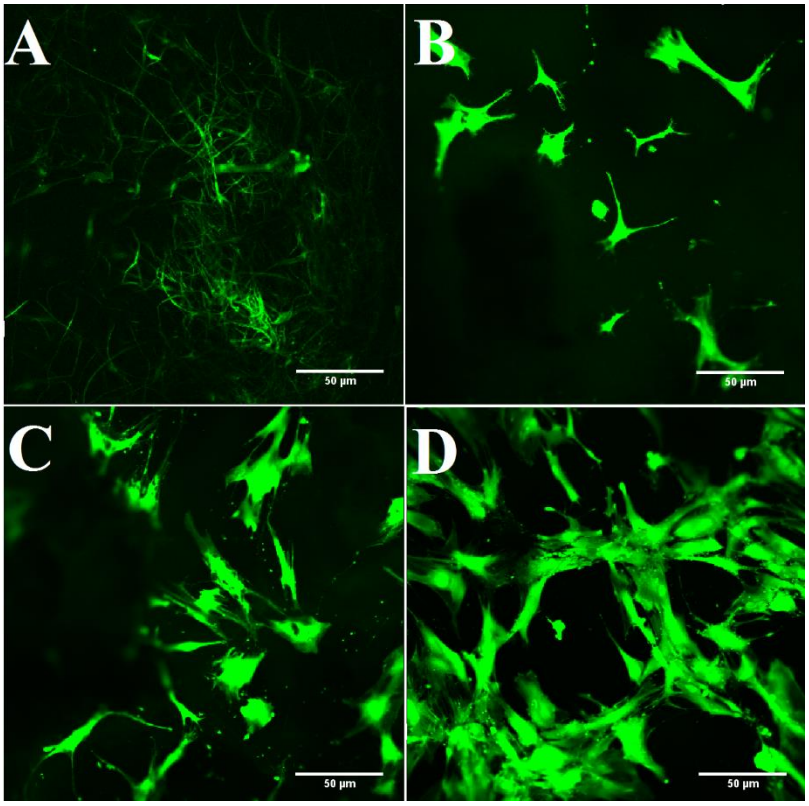

FIG. 10. Non-treated groups are analyzed using confocal microscopy at 10X magnification at day 14. It can be observed that the PCL/CA group in part (A), the PCL/CA+CHT group in part (B), the PCL/CA+CHT/LS group in part (C), and the PCL/CA+CHT/SPANI group in part (D) are supportive of cell attachment and viability. It should be noted, however, that the PCL/CA+CHT group was found to be significantly less supportive of cell attachment in comparison to other groups.

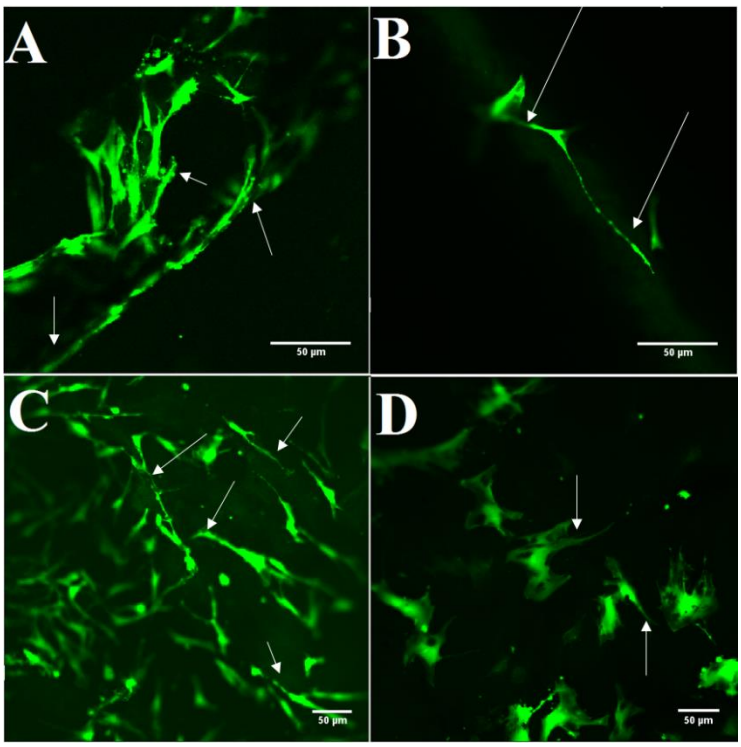

FIG. 11. Samples treated with NGF are analyzed using confocal microscopy at 10X or 20X magnification at day 14. Once again, part (A) represents the PCL/CA group, part (B) represents the PCL/CA+CHT group, part (C) represents the PCL/CA+CHT/LS group, and part (D) represents the PCL/CA+CHT/SPANI group. In comparison to figure 9, greater neurite extension can be noted and is indicated by arrows.

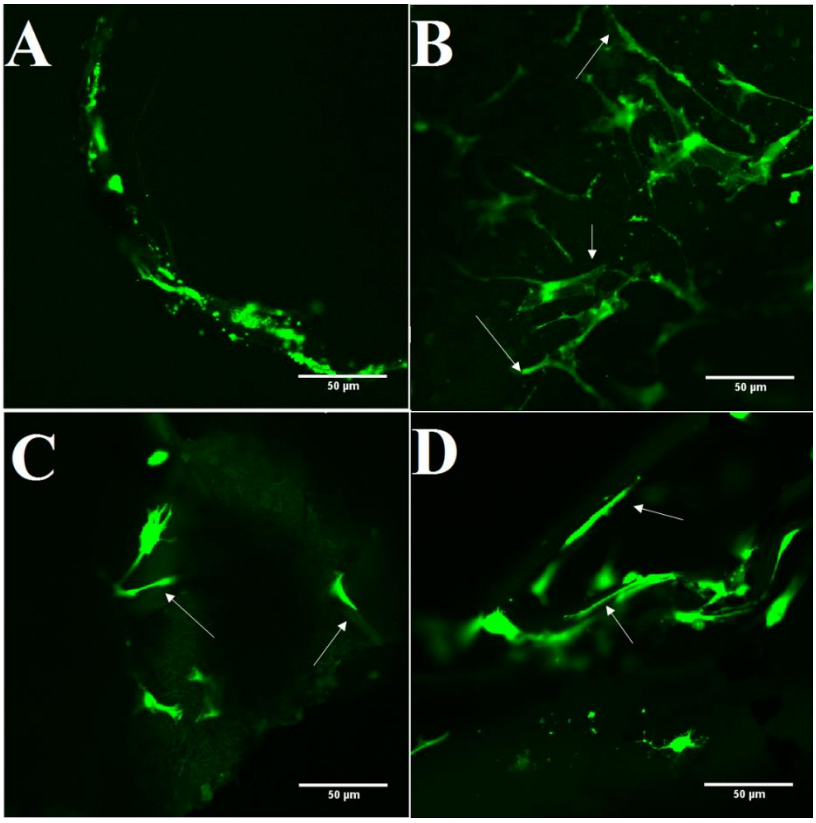

FIG. 12. Samples treated with ES at 1V are analyzed using confocal microscopy at 10X magnification at day 11. Once again, part (A) represents the PCL/CA group, part (B) represents the PCL/CA+CHT group, part (C) represents the PCL/CA+CHT/LS group, and part (D) represents the PCL/CA+CHT/SPANI group. In comparison to figure 9, greater neurite extension can be noted and is indicated by arrows.

3.2.2 Cell differentiation

It has been speculated that hMSCs may differentiate into Schwann cell-like lineages in the presence of conductive polymers and ES (*64*). This is incredibly important for *in vivo* nerve regeneration applications, where ES has been shown to both bridge nerve gaps beyond biological limits and guide axonal outgrowth in one particular direction (*29*). Thus, as mentioned previously, undifferentiated hMSCs seeded onto a conduit aid in macrophage recruitment, while differentiated Schwann cells under the influence of ES form the bands of Büngner in order to further accelerate nerve gap repair (*58, 60*).

In order to analyze the presence of neuronal protein marker β-III tubulin, scaffolds were stained with anti β-III tubulin antibody and observed using confocal microscopy at day 14 for

both NGF and ES groups. From observation of both *figures 13* and *14*, positive staining can be observed in both groups. Thus, while there is little cellular attachment beyond day 11 in ES groups, positive staining for β-III tubulin at day 14 does indicate that differentiation occurred over the time period.

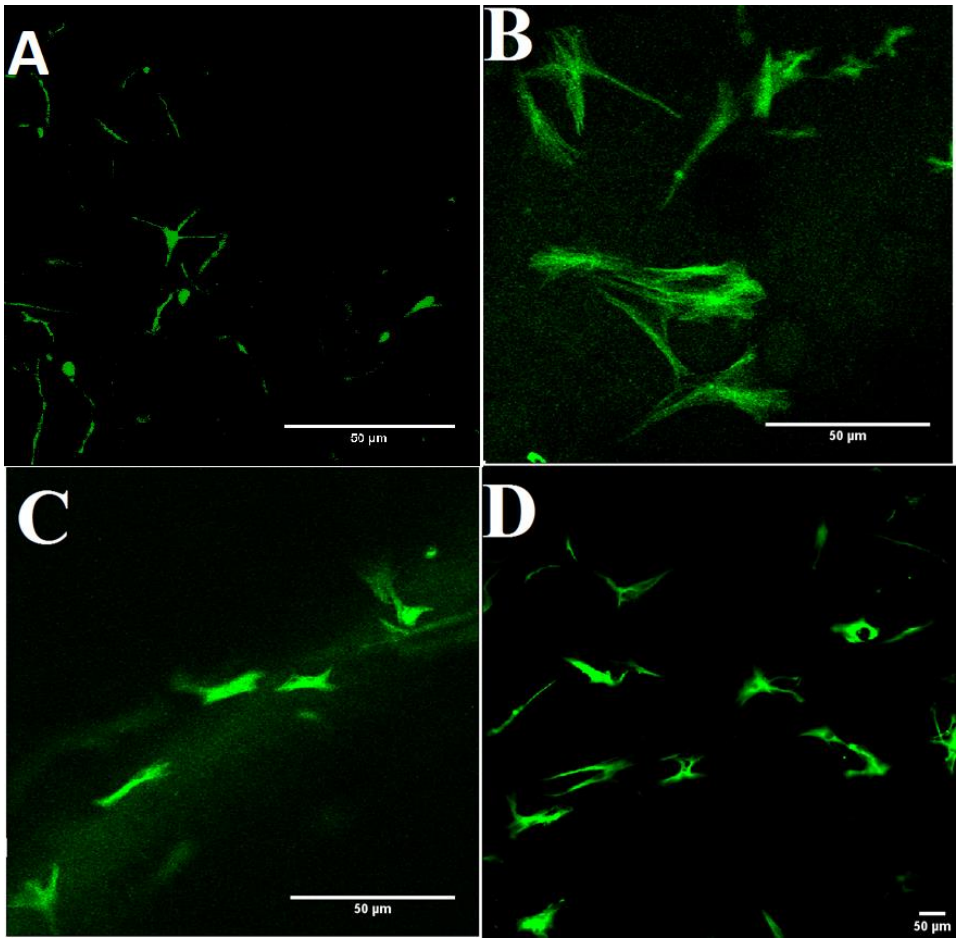

FIG. 13. Samples treated with NGF are observed at day 14 after incubation with anti-βIII tubulin antibody. Images are taken using confocal microscopy at 10X or 20X magnification. Part (A) represents the PCL/CA group, part (B) represents the PCL/CA+CHT group, part (C) represents the PCL/CA+CHT/LS group, and part (D) represents the PCL/CA+CHT/SPANI group. It can be observed that the hydrogel coated groups demonstrate a less acute fluorescence in comparison to the PCL/CA nanofiber group, most likely due to the fact that surface irregularities are present. Arrows indicate cell bodies.

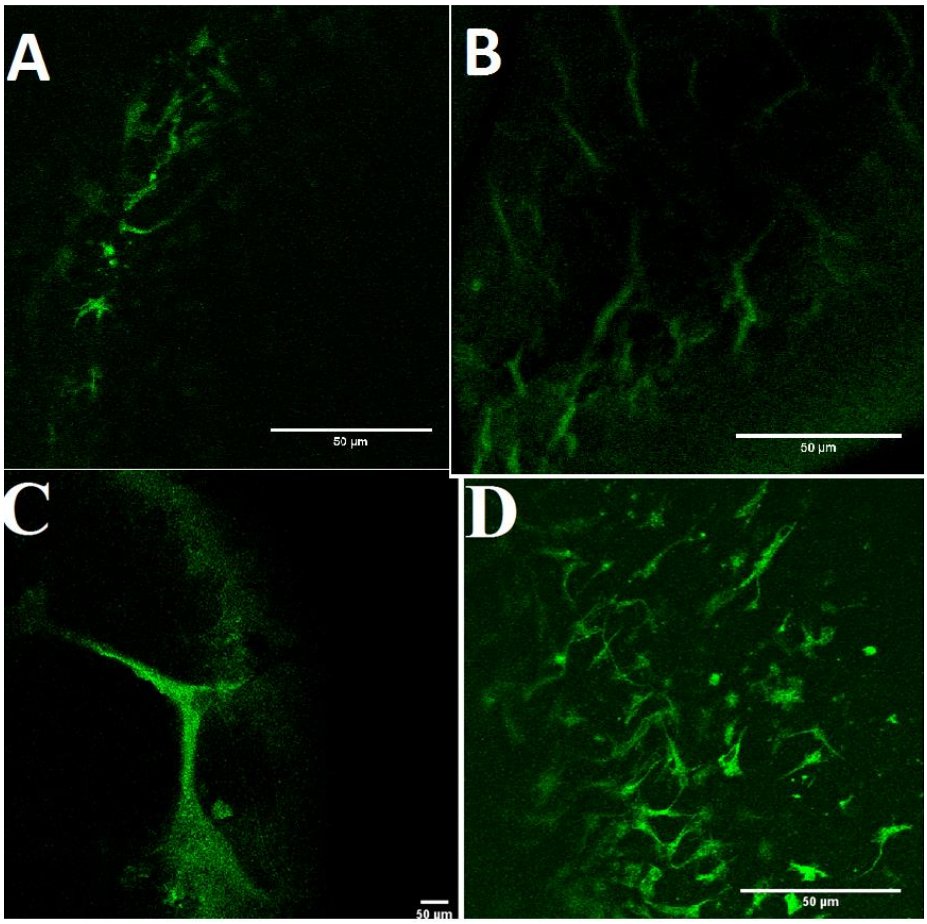

FIG. 14. Samples treated with ES are observed at day 14 after incubation with anti-βIII tubulin antibody. Images are taken using confocal microscopy at 10X or 20X magnification. Part (A) represents the PCL/CA group, part (B) represents the PCL/CA+CHT group, part (C) represents the PCL/CA+CHT/LS group, and part (D) represents the PCL/CA+CHT/SPANI group. It can be observed that the hydrogel coated groups demonstrate a less acute fluorescence in comparison to the PCL/CA nanofiber group, most likely due to the fact that surface irregularities are present. Arrows indicate cell bodies.

3.2.3 Cell proliferation

It is well established that there is an inverse relationship between differentiation and proliferation – when cells are proliferating, little differentiation is expected and vise-versa (*65*). Therefore, there should be nearly negligible proliferation observed for ES treated cells over a 14 day period. Observation of *figure 15* shows a cellular proliferation profile that is nearly constant within standard error for PCL/CA, PCL/CA+CHT, and PCL/CA+CHT/LS groups. Interestingly, PCL/CA+CHT/SPANI does demonstrate the most superior and noticeable proliferation profile, coinciding with a greater concentration of β-III tubilin present on the scaffold treated with ES.

This is most likely due to the greater hydrophilicity – and in turn greater cellular attachment, of SPANI in comparison to PCL/CA, CHT, and LS.

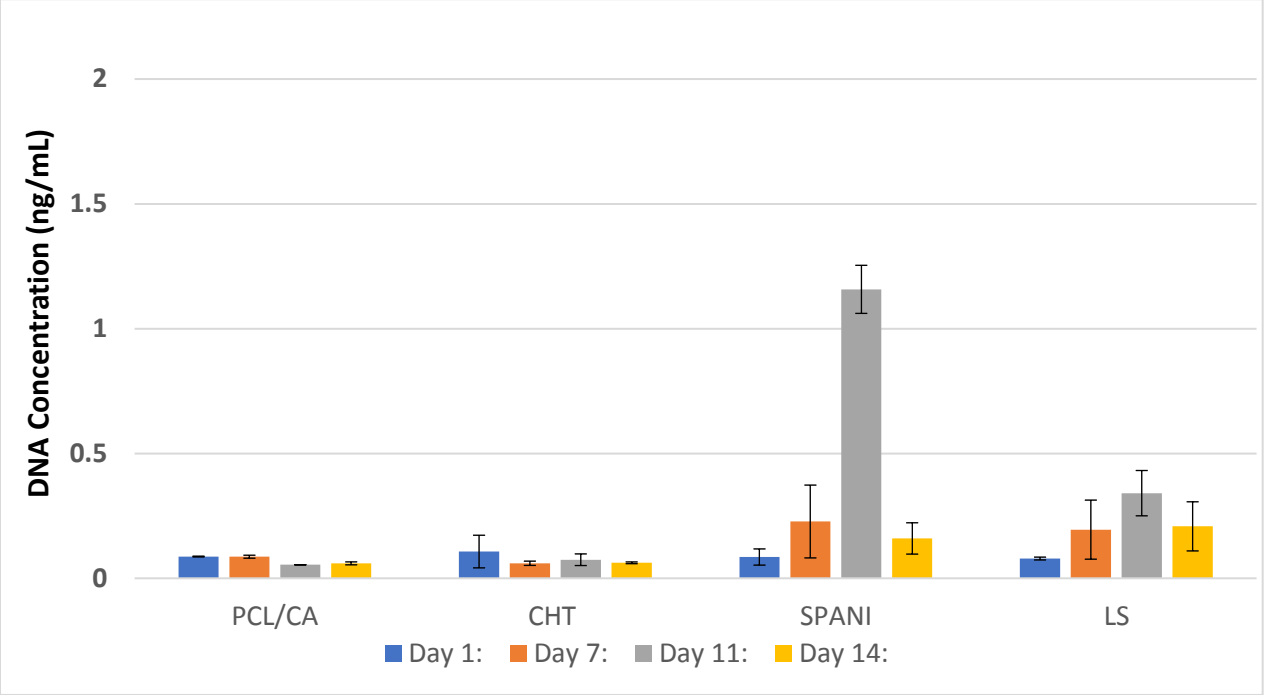

FIG. 15. Cellular proliferation rate is nearly 0 for ES treated scaffold groups with the exception of PCL/CA+CHT/SPANI, most likely due to the greater hydrophilicity of the scaffold leading to superior cell attachment. *Indicates $p<0.05$ versus PCL/CA.

4. Conclusions

Morphologically, the fabricated composite structures demonstrated both an interconnected porous core with randomly orientated nanofibers and a conductive hydrogel layer. The polymeric composites stabilized after a two-week period in physiological conditions, retaining most of their conductivity. Following incubation in physiological conditions overnight, tensile properties revealed brittle nature in hydrogel groups and an elastic nature in the PCL/CA nanofiber group, as is to be expected. The presence of SPANI and LS led to less tensile strength due to the hydrophilicity of the materials allowing for greater aqueous infiltration and thus pre-stretching of the fibers. For *in vitro* cell studies, cellular attachment was observed in all groups

for at least an 11-day period, and up to a 14 day period for NGF and non-treated scaffold groups. Immunohistochemistry staining for β-III tubulin protein marker revealed qualitatively dense concentrations of the protein in all groups at 14 days, with the PCL/CA+CHT/SPANI group demonstrating the greatest concentration with the images shown. The extra hydrophilicity of the scaffold most likely created an environment for superior cellular attachment, and thus greater differentiation. However, this has yet to be confirmed via blotting. While β-III tubulin was retained in all ES treated groups at day 14, a PicoGreen dsDNA assay revealed little proliferation in these groups, coinciding with live/dead staining demonstrating little to no cells at day 14 (not shown). The presence of cells at day 11, however, should be sufficient for macrophage and schwann cell recruitment, nutrient transportation, and ultimately bands of Büngner formation. Further optimization of ES parameters and material fabrication techniques should be utilized in future studies in order to maximize cellular attachment, proliferation and viability.

References

1. J. Noble, C. A. Munro, V. S. Prasad, R. Midha, Analysis of upper and lower extremity peripheral nerve injuries in a population of patients with multiple injuries. *Journal of Trauma and Acute Care Surgery* **45**, 116-122 (1998).
2. L. R. Robinson, Traumatic injury to peripheral nerves. *Muscle & nerve* **23**, 863-873 (2000).
3. X. Jiang, S. H. Lim, H.-Q. Mao, S. Y. Chew, Current applications and future perspectives of artificial nerve conduits. *Experimental neurology* **223**, 86-101 (2010).
4. M. Deng, R. James, C. T. Laurencin, S. G. Kumbar, Nanostructured polymeric scaffolds for orthopaedic regenerative engineering. *NanoBioscience, IEEE Transactions on* **11**, 3-14 (2012).
5. S. Kehoe, X. Zhang, D. Boyd, FDA approved guidance conduits and wraps for peripheral nerve injury: a review of materials and efficacy. *Injury* **43**, 553-572 (2012).
6. D. Grinsell, C. Keating, Peripheral nerve reconstruction after injury: a review of clinical and experimental therapies. *BioMed research international* **2014**, (2014).
7. S. Madduri, M. Papaloizos, B. Gander, Trophically and topographically functionalized silk fibroin nerve conduits for guided peripheral nerve regeneration. *Biomaterials* **31**, 2323-2334 (2010).
8. A. R. Nectow, K. G. Marra, D. L. Kaplan, Biomaterials for the development of peripheral nerve guidance conduits. *Tissue Engineering Part B: Reviews* **18**, 40-50 (2011).
9. Y.-t. Kim, M. I. Romero-Ortega, Material considerations for peripheral nerve interfacing. *Mrs Bulletin* **37**, 573-580 (2012).
10. S. Madduri, B. Gander, Growth factor delivery systems and repair strategies for damaged peripheral nerves. *Journal of Controlled Release* **161**, 274-282 (2012).

11. J. Xie *et al.*, Nerve guidance conduits based on double-layered scaffolds of electrospun nanofibers for repairing the peripheral nervous system. *ACS applied materials & interfaces* **6**, 9472-9480 (2014).
12. Y. Wang *et al.*, Electrospun, Reinforcing Network-Containing, Silk Fibroin-Based Nerve Guidance Conduits for Peripheral Nerve Repair. *Journal of Biomaterials and Tissue Engineering* **6**, 53-60 (2016).
13. B.-K. Lee *et al.*, End-to-side neurorrhaphy using an electrospun PCL/collagen nerve conduit for complex peripheral motor nerve regeneration. *Biomaterials* **33**, 9027-9036 (2012).
14. R. James, S. G. Kumbar, C. T. Laurencin, G. Balian, A. B. Chhabra, Tendon tissue engineering: adipose-derived stem cell and GDF-5 mediated regeneration using electrospun matrix systems. *Biomedical materials (Bristol, England)* **6**, 025011 (2011).
15. N. B. Shelke *et al.*, Neural tissue engineering: nanofiber-hydrogel based composite scaffolds. *Polymers for Advanced Technologies* **27**, 42-51 (2016).
16. M. G. Yeo, G. H. Kim, Preparation and characterization of 3D composite scaffolds based on rapid-prototyped PCL/β-TCP struts and electrospun PCL coated with collagen and HA for bone regeneration. *Chemistry of Materials* **24**, 903-913 (2011).
17. P. Balasubramanian, J. A. Roether, D. W. Schubert, J. P. Beier, A. R. Boccaccini, Bi-layered porous constructs of PCL-coated 45S5 bioactive glass and electrospun collagen-PCL fibers. *Journal of Porous Materials* **22**, 1215-1226 (2015).
18. F. A. Müller *et al.*, Cellulose-based scaffold materials for cartilage tissue engineering. *Biomaterials* **27**, 3955-3963 (2006).
19. B. Cecen *et al.*, Biocompatibility and biomechanical characteristics of loofah based scaffolds combined with hydroxyapatite, cellulose, poly-l-lactic acid with chondrocyte-like cells. *Materials Science and Engineering: C* **69**, 437-446 (2016).
20. K. Haastert-Talini, C. Grothe, Electrical stimulation for promoting peripheral nerve regeneration. *Int Rev Neurobiol* **109**, 111-124 (2013).
21. A. N. Koppes *et al.*, Electrical stimulation of Schwann cells promotes sustained increases in neurite outgrowth. *Tissue Engineering Part A* **20**, 494-506 (2013).
22. X. Gu *et al.*, Low-frequency electrical stimulation induces the proliferation and differentiation of peripheral blood stem cells into schwann cells. *The American journal of the medical sciences* **349**, 157-161 (2015).
23. C. Witzel, T. M. Brushart, G. Koulaxouzidis, M. Infanger, Electrical Nerve Stimulation Enhances Perilesional Branching after Nerve Grafting but Fails to Increase Regeneration Speed in a Murine Model. *Journal of reconstructive microsurgery*, (2016).
24. Y. J. Chang, C. M. Hsu, C. H. Lin, M. S. Lu, L. Chen, Electrical stimulation promotes nerve growth factor-induced neurite outgrowth and signaling. *Biochimica et biophysica acta* **1830**, 4130-4136 (2013).
25. K. Lee, E. A. Silva, D. J. Mooney, Growth factor delivery-based tissue engineering: general approaches and a review of recent developments. *Journal of the Royal Society Interface* **8**, 153-170 (2011).
26. D. Kai, S. Jiang, Z. W. Low, X. J. Loh, Engineering highly stretchable lignin-based electrospun nanofibers for potential biomedical applications. *Journal of Materials Chemistry B* **3**, 6194-6204 (2015).
27. Y. Yang *et al.*, Synthesis and characterization of cytocompatible sulfonated polyanilines. *Macromolecular rapid communications* **32**, 887-892 (2011).
28. M. Bellot *et al.*, Dual agonist occupancy of AT1-R-α2C-AR heterodimers results in atypical Gs-PKA signaling. *Nat Chem Biol* **11**, 271-279 (2015).

29. K. Elzinga *et al.*, Brief electrical stimulation improves nerve regeneration after delayed repair in Sprague Dawley rats. *Experimental neurology* **269**, 142-153 (2015).
30. H. T. Nguyen *et al.*, Electric field stimulation through a substrate influences Schwann cell and extracellular matrix structure. *Journal of neural engineering* **10**, 046011 (2013).
31. A. Cipitria, A. Skelton, T. Dargaville, P. Dalton, D. Hutmacher, Design, fabrication and characterization of PCL electrospun scaffolds—a review. *Journal of Materials Chemistry* **21**, 9419-9453 (2011).
32. Y. Zhang, J. Venugopal, Z.-M. Huang, C. Lim, S. Ramakrishna, Characterization of the surface biocompatibility of the electrospun PCL-collagen nanofibers using fibroblasts. *Biomacromolecules* **6**, 2583-2589 (2005).
33. J. Cai *et al.*, Thermal properties and crystallization behavior of thermoplastic starch/poly (ε-caprolactone) composites. *Carbohydrate polymers* **102**, 746-754 (2014).
34. H. Yu, Y. Jia, C. Yao, Y. Lu, PCL/PEG core/sheath fibers with controlled drug release rate fabricated on the basis of a novel combined technique. *International journal of pharmaceutics* **469**, 17-22 (2014).
35. R. Safaeijavan, M. Soleimani, A. Divsalar, A. Eidi, A. Ardeshirylajimi, Biological behavior study of gelatin coated PCL nanofiberous electrospun scaffolds using fibroblasts. *Journal of Paramedical Sciences* **5**, (2013).
36. D. Zavastin *et al.*, Preparation, characterization and applicability of cellulose acetate–polyurethane blend membrane in separation techniques. *Colloids and Surfaces A: Physicochemical and Engineering Aspects* **370**, 120-128 (2010).
37. L. L. Fernandes *et al.*, Cytocompatibility of chitosan and collagen-chitosan scaffolds for tissue engineering. *Polimeros* **21**, 1-6 (2011).
38. K. M. Gregorio-Jauregui *et al.*, One-step method for preparation of magnetic nanoparticles coated with chitosan. *Journal of Nanomaterials* **2012**, 4 (2012).
39. L. C. Mendes, A. P. S. Falco, M. S. Pinho, P. O. Marques, Sulfonated polyaniline: influence of sulfonation routes on its thermal and structural characteristics. *Materials Research* **14**, 466-471 (2011).
40. F. M. Watt, W. T. Huck, Role of the extracellular matrix in regulating stem cell fate. *Nature reviews Molecular cell biology* **14**, 467-473 (2013).
41. P. Kolhe, R. M. Kannan, Improvement in ductility of chitosan through blending and copolymerization with PEG: FTIR investigation of molecular interactions. *Biomacromolecules* **4**, 173-180 (2003).
42. R. R. Duling, R. B. Dupaix, N. Katsube, J. Lannutti, Mechanical characterization of electrospun polycaprolactone (PCL): a potential scaffold for tissue engineering. *Journal of Biomechanical Engineering* **130**, 011006 (2008).
43. E. P. De Azevedo, Chitosan hydrogels for drug delivery and tissue engineering applications. *International Journal of Pharmacy and Pharmaceutical Sciences* **7**, 8-14 (2015).
44. C. Pang, R. A. Shanks, F. Daver, Characterization of kenaf fiber composites prepared with tributyl citrate plasticized cellulose acetate. *Composites Part A: Applied Science and Manufacturing* **70**, 52-58 (2015).
45. T. Gordon, Electrical stimulation to enhance axon regeneration after peripheral nerve injuries in animal models and humans. *Neurotherapeutics* **13**, 295-310 (2016).
46. K. Lee, E. A. Silva, D. J. Mooney, Growth factor delivery-based tissue engineering: general approaches and a review of recent developments. *Journal of the Royal Society, Interface* **8**, 153-170 (2011).
47. M. B. Runge *et al.*, The Development of Electrically Conductive Polycaprolactone Fumarate-Polypyrrole Composite Materials for Nerve Regeneration. *Biomaterials* **31**, 5916-5926 (2010).

48. M. Chipara, K. Lozano, A. Hernandez, M. Chipara, TGA analysis of polypropylene–carbon nanofibers composites. *Polymer Degradation and Stability* **93**, 871-876 (2008).
49. A. George *et al.*, Design of low-cost ionic liquids for lignocellulosic biomass pretreatment. *Green Chemistry* **17**, 1728-1734 (2015).
50. M. Zanetti, V. Causin, R. Saini, A. Cardin, R. Cavalli, Effect of tannin on increasing UF adhesive performance at high temperature investigated by TMA and TGA analysis. *European Journal of Wood and Wood Products* **72**, 385-392 (2014).
51. M. Siddique, M. Amin, Thermogravimetric Analysis (TGA) of Lignite Coal, Tree Leaves and Their blend. *Journal of Applied and Emerging Sciences* **4**, pp118-121 (2016).
52. E. S. Gil, S.-H. Park, X. Hu, P. Cebe, D. L. Kaplan, Impact of Sterilization on the Enzymatic Degradation and Mechanical Properties of Silk Biomaterials. *Macromolecular Bioscience* **14**, 257-269 (2014).
53. J. Kolmas, M. Szwaja, W. Kolodziejski, Solid-state NMR and IR characterization of commercial xenogeneic biomaterials used as bone substitutes. *Journal of Pharmaceutical and Biomedical Analysis* **61**, 136-141 (2012).
54. T. Jacobs *et al.*, Improved cell adhesion to flat and porous plasma-treated poly-ε-caprolactone samples. *Surface and Coatings Technology* **232**, 447-455 (2013).
55. N. Liao *et al.*, Electrospun bioactive poly (ε-caprolactone)–cellulose acetate–dextran antibacterial composite mats for wound dressing applications. *Colloids and Surfaces A: Physicochemical and Engineering Aspects* **469**, 194-201 (2015).
56. E. Martínez-Campos *et al.*, Cell Adhesion and Proliferation on Sulfonated and Non-Modified Chitosan Films. *AAPS PharmSciTech*, 1-9 (2016).
57. P. Bober, P. Humpolíček, J. Pacherník, J. Stejskal, T. Lindfors, Conducting polyaniline based cell culture substrate for embryonic stem cells and embryoid bodies. *RSC Advances* **5**, 50328-50335 (2015).
58. L. Chen, E. E. Tredget, P. Y. Wu, Y. Wu, Paracrine factors of mesenchymal stem cells recruit macrophages and endothelial lineage cells and enhance wound healing. *PloS one* **3**, e1886 (2008).
59. G. R. D. Evans *et al.*, Bioactive poly(l-lactic acid) conduits seeded with Schwann cells for peripheral nerve regeneration. *Biomaterials* **23**, 841-848 (2002).
60. A. Rajaram, (2015).
61. W. Ge *et al.*, Differentiation of Mesenchymal Stem Cells into Neural Stem Cells Using Cerebrospinal Fluid. *Cell biochemistry and biophysics* **71**, 449-455 (2015).
62. K. Gunther, A. Appelt-Menzel, C. K. Kwok, H. Walles, M. Metzger, Rapid Monolayer Neural Induction of induced Pluripotent Stem Cells Yields Stably Proliferating Neural Stem Cells. *Journal of Stem Cell Research & Therapy* **2016**, (2016).
63. Y.-C. Cheng *et al.*, Microfluidic platform for human placenta-derived multipotent stem cells culture and applied for enhanced neuronal differentiation. *Microfluidics and Nanofluidics* **18**, 587-598 (2015).
64. W. Guo *et al.*, Self-powered electrical stimulation for enhancing neural differentiation of mesenchymal stem cells on graphene-poly (3, 4-ethylenedioxythiophene) hybrid microfibers. *ACS nano* **10**, 5086-5095 (2016).
65. S. Ruijtenberg, S. van den Heuvel, Coordinating cell proliferation and differentiation: Antagonism between cell cycle regulators and cell type-specific gene expression. *Cell Cycle* **15**, 196-212 (2016).